euspen's 26th International Conference & Exhibition, Krakow, PL, June 2026
www.euspen.eu

Control system modeling for a micro machining spindle with an active magnetic bearing actuator

Felix Zell[1], Maximilian Vierling[1], Jan C. Aurich[1]

[1]*University of Kaiserslautern-Landau, Institute for Manufacturing Technology and Production Systems*

felix.zell@rptu.de

Abstract
In micro machining, achieving high surface quality and extending tool life requires minimizing spindle vibrations across a wide speed range. Air bearing spindles, commonly used for their high precision, lack active control capabilities and are therefore unable to compensate speed-dependent excitations, such as unbalance or cutting forces, and ambient disturbances. Active magnetic bearing spindles provide active vibration control but are rarely used in micro machining due to their complexity and cost. Combining an air bearing spindle with a single active magnetic bearing offers a practical solution to achieve vibration suppression with reduced system complexity.
This paper presents a model of a closed-loop control system for such a hybrid spindle concept that combines an air bearing with one active magnetic bearing. The air bearing stiffness and damping coefficients and the electromagnetic bearing forces are calculated via finite element simulations prior to use in the control loop. They are implemented in the control system via lookup tables to enable realistic system behavior with low computational costs. The system dynamics (e.g. the rotor movement) are computed as functions of the air bearing forces, the electromagnetic force, the motor torque and the unbalance forces.
The vibration response of the spindle is analyzed for operating speeds between 25 000 min^{-1} and 125 000 min^{-1}. The results show that the closed-loop control system can significantly suppress vibrations up to 60 000 min^{-1}, while at higher speeds the system remains stable without notable damping.
These findings demonstrate the potential of hybrid spindle systems to improve vibration performance in micro machining applications and provide a modeling framework for further development of advanced control strategies.

Micro machining, Control, Magnetic bearing, Mechatronic

1. Introduction

Achieving high surface quality in micro milling requires precision spindles, as even minor vibrations can compromise dimensional accuracy and tool life [1, 2]. Due to the small tool diameters, very high spindle speeds are needed to ensure sufficient cutting speeds. At the same time, the undeformed chip thickness is extremely small, which makes the process highly sensitive to dynamic effects. Spindle vibrations, tool run-out, and dynamic compliance are among the dominant limiting factors for surface quality, dimensional accuracy, and tool life in micro milling [1].

For micro machining applications, air bearing spindles are widely used due to their low friction, high rotational accuracy, and suitability for compact machine tools [3]. However, air bearing spindles are inherently passive systems and therefore highly sensitive to disturbances such as rotor unbalance, air supply pressure fluctuations, and electromagnetic motor forces. Sun et al. [4] demonstrated that such disturbances cause periodic spindle vibrations that transfer to the machined surface, resulting in waviness and lower surface quality.

Active magnetic bearings enable the active compensation of disturbing forces by controlling rotor position, stiffness, and damping in real time. Their potential for vibration suppression and stability enhancement in high-speed spindles for micro machining has been demonstrated by Kimman et al. [5].

A less complex and cheaper alternative is the combination of air bearings with a single active magnetic bearing in a hybrid spindle concept. Jang et al. [6] showed that such a hybrid aerostatic bearing–rotor system allows a significant increase in the maximum stable rotational speed up to 35 000 min^{-1} by actively suppressing self-excited whirl and pneumatic-hammer instabilities.

These studies highlight the potential of active magnetic bearing spindles for micro machining and research efforts towards hybrid spindle systems for high speed applications. However, a comprehensive model of hybrid spindles for micro machining, that accounts for nonlinearities and small geometric dimensions, is not yet available. Such a model must incorporate realistic air bearing characteristics, magnetic bearing forces, rotor unbalance, motor torque, and speed-dependent system dynamics to achieve high simulation accuracy.

This paper presents a closed-loop control system model for a hybrid micro machining spindle combining an air bearing spindle with a single active magnetic bearing actuator. The air bearing stiffness and damping as well as the electromagnetic bearing forces are obtained from finite element simulations and implemented using lookup tables for computational efficiency. The rotor dynamics are simulated as a function of air bearing forces, electromagnetic control forces, motor torque, and unbalance excitation. The vibration behavior is analyzed for rotational speeds between 25 000 min^{-1} and 125 000 min^{-1}, demonstrating the vibration suppression capability and stability of the hybrid concept over a wide operating range.

2. Methods

The model of the closed-loop control system of the hybrid spindle is set up as a time-dependent model with three degrees of freedom (positions x and y and angle about the z-axis φ) in MATLAB[1] Simulink R2024b – see figure 1. Two radial aerostatic bearings in addition of one radial magnetic bearing make up the hybrid spindle. The three corresponding equations of motions for the rotordynamics define the plant of the closed-loop system with the rotor mass m , the rotor eccentricity ε the rotor's moment of inertia about the z-axis J, the rotor positions, velocities and accelerations $x, y, \dot{x}, \dot{y}, \ddot{x}, \ddot{y}$, the rotational angle, velocity and acceleration $\varphi, \dot{\varphi}, \ddot{\varphi}$, the magnetic bearing forces $F_{MB,x}$ and $F_{MB,y}$, the air bearing forces $F_{AB,x}$ and $F_{AB,y}$ and the motor torque M:

$$m\ddot{x} = F_{MB,x} - F_{AB,x} + m \cdot \varepsilon \cdot \dot{\varphi}^2 \cdot \cos\varphi \tag{1}$$

$$m\ddot{y} = F_{MB,y} - F_{AB,y} + m \cdot \varepsilon \cdot \dot{\varphi}^2 \cdot \sin\varphi \tag{2}$$

$$\begin{aligned} J\ddot{\varphi} = M &+ (y + \varepsilon \cdot \sin\varphi) \cdot (F_{MB,x} - F_{AB,x}) \\ &+ (x + \varepsilon \cdot \cos\varphi) \cdot (-F_{MB,y} + F_{AB,y}) \end{aligned} \tag{3}$$

The air bearing forces and the magnetic bearing forces are computed numerically before implementing them into the control loop model via lookup tables. This ensures realistic system behavior with low computational cost.

2.1. Calculation of air bearing forces

The air bearing forces of the investigated aerostatic air bearing spindle can be calculated based on their damping and stiffness coefficients c_{ij} and k_{ij} and the instantaneous positions and velocities $(x, \dot{x}, y, \dot{y})$:

$$F_{AB,x} = c_{xx} \cdot \dot{x} + c_{xy} \cdot \dot{y} + k_{xx} \cdot x + k_{xy} \cdot y \tag{4}$$

$$F_{AB,y} = -c_{xy} \cdot \dot{x} + c_{xx} \cdot \dot{y} - k_{xy} \cdot x + k_{xx} \cdot y \tag{5}$$

The damping and stiffness coefficients are a function of the spindle speed and are calculated numerically. We used the precision air bearing simulator PABS, which is a 2D fluid dynamics simulation tool developed at our institute [7] based on the thin-film theory to simulate the two radial air bearings separatly. The resulting damping and stiffness coefficients are added for implementation in the control model. The inputs for the simulation and the resultant air bearing coefficients are given in table 1 and 2 respectively:

Table 1. Inputs for air bearing coefficient calculation

Parameter	Bearing 1	Bearing 2	Unit
air bearing gap in	18.5	16	10^{-6} m
number of nozzles	8	8	-
nozzle diameter in	0.035	0.035	10^{-3} m
supply air pressure in	6	6	10^{5} N/m²
bearing length in	34.4	28.2	10^{-3} m
bearing diameter in	20.7	20.7	10^{-3} m
discharge coefficient c_d	1	1	-
relative eccentricity	0.1	0.1	-

Table 2. Resultant damping and stiffness coefficients

Spindle speed	Direct stiffness	Cross-coupled stiffness	Direct damping	Cross-coupled damping
n in min^{-1}	k_{xx} in $\frac{MN}{m}$	k_{xy} in $\frac{MN}{m}$	c_{xx} in $\frac{kNs}{m}$	c_{xy} in $\frac{kNs}{m}$
1 500	4.540	0.194	0.769	-0.169
25 000	7.246	1.273	1.633	-0.738
50 000	9.919	0.088	0.922	0.052
75 000	11.582	-0.739	0.595	0.212
100 000	12.725	-1.151	0.412	0.162
125 000	13.542	-1.335	0.300	0.069

These damping and stiffness coefficients are implemented in the control loop via 1D lookup tables.

2.2. Calculation of magnetic bearing forces

The magnetic bearing forces are calculated in a three dimensional magnetostatic finite element (FE) simulation using ANSYS[1] Mechanical 2021R2. The parameters of the simulated heteropolar 4 pole-pair active magnetic bearing with differential driving scheme are given in table 3. For detailed information on the FE-model setup we refer to [8].

Table 3. Simulation input data

Parameter	Value	Unit
magnetic bearing gap s_0	0.3	10^{-3} m
bias current i_0	3	A
maximum control current i_c	±2.5	A
coil height	3	10^{-3} m
coil length	10.6	10^{-3} m
coil width	6.1	10^{-3} m
number of coil windings	50	-
inner stator diameter	16	10^{-3} m
outer stator diameter	30.2	10^{-3} m
saturation flux density stator	1.55*	T

* magnetic properties implemented as non-linear BH-curve

Each simulation run calculates the magnetic bearing forces for a given rotor position in x and y for 121 combinations of control currents i_{cx}, i_{cy} in the range of -2.5 A to +2.5 A with a step size of 0.5 A. The results for the magnetic bearing forces $F_{MB,x}$ and

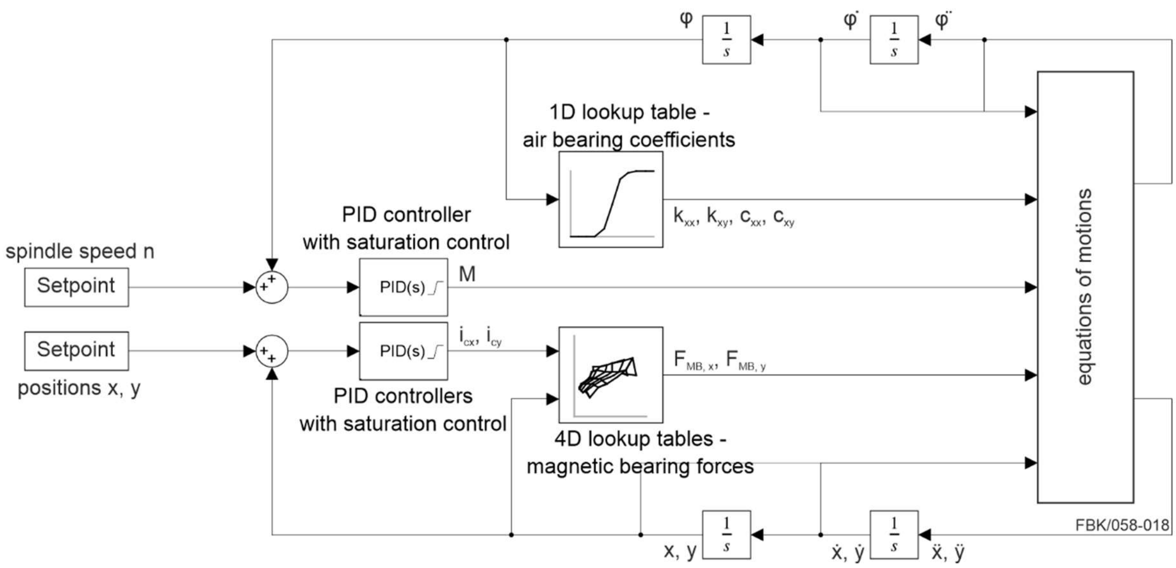

Figure 1. Scheme of the closed loop control system of the hybrid spindle

$F_{MB,y}$ are gathered in 4D lookup tables for implementation in the control loop. There the current rotor position in x and y combined with the currents i_x and i_y are used to extract the corresponding magnetic bearing force from the lookup table.

2.3. Control system simulation

The control system is set up to enable setpoint tracking of the rotor position x, y and the rotational velocity $\dot{\varphi}$ – see figure 1. For the position control the instantaneos difference of the rotor position from the setpoint is fed into single input, single output proportional-integral-derivative (PID) controllers to determine the necessary control currents i_c. Together with the current rotor position these four signals are used to evaluate the corresponding magnetic bearing forces from the 4D lookup tables. For the air bearing forces the damping and stiffness coeffecients are evaluated from the 1D lookup tables based on the current rotational velocity. The magnetic bearing forces, the air bearing coeffecients and the current positions and velocities $x, y, \dot{x}, \dot{y}$ are used to solve equations of motion for the updated accelerations $\ddot{x}, \ddot{y}$. Integrating these twice provide the system with the updated velocities and positions $\dot{x}, \dot{y}$ and x, y, respectively. For control of the rotational velocity, the instantaneous difference from the setpoint value is fed into a single input, single output PID-controller with saturation control to determine the necessary motor torque. This motor torque together with the current bearing forces, rotor positons and velocities is used to solve the equation of motion (3) for the updated rotational acceleration $\ddot{\varphi}$ and in turn the rotational velocity $\dot{\varphi}$. The controller parameters for the rotor position controllers are optimized using the automated MATLAB Simulink 'PID Tuner App' based on the step response of the linearized plant. An overview of input parameters is given in table 4.

Table 4. Control system input data

Parameter	Value	Unit
step size - fixed	$1 \cdot 10^{-6}$	s
solver	ode3	-
simulation time	0.2	s
rotor mass m	0.315	kg
rotor's moment of inertia about z-axis J	$2.1 \cdot 10^{-5}$	kgm²
rotor eccentricity ε	$1.5 \cdot 10^{-6}$	m
maximum motor torque M	1.5	Nm

3. Results

To evaluate the potential of the hybrid spindle concept, two different load scenarios are investigated for the operating range of the air bearing spindle (spindle speeds from 25 000 min^{-1} to 125 000 min^{-1}).

I. Actuator inactive and position setpoints set to 0 at constant spindle speeds. These results are used to validate the system dynamics by comparing them to measured vibration amplitudes of the uncontrolled air bearing spindle [9].
II. Actuator active and position setpoints set to 0 at constant spindle speeds. This scenario corresponds to a free spinning rotor with active vibration control.

The analysis of the hybrid spindle performance is based on a comparison of the simulated responses of the uncontrolled (I) and controlled (II) systems.

The combined results of scenarios I and II are shown as peak-to-peak values of the rotor amplitudes as a function of spindle speeds in figure 2. Since the rotor dynamics, as well as the air and magnetic bearing forces used as input variables, show equivalent results in the x- and y-directions, the results are discussed using the x-direction only. The peak-to-peak values for the experimental data rise from 2.7 µm to 4.4 µm at 30 000 min^{-1} and 125 000 min^{-1}, respectively. A local maximum was found at 80 000 min^{-1} and 3.9 µm. However, the simulated vibration amplitudes without vibration control reach a maximum of 13.3 µm at 35 000 min^{-1}, most likely due to matching a natural frequency. Subsequently the vibration amplitudes drop to 4 µm at 65 000 min^{-1} and keep decreasing to 3.2 µm at 125 000 min^{-1}. Overall the simulated rotor dynamics closely match the real rotor dynamics in the range of 65 000 min^{-1} to 110 000 min^{-1} and overestimate the vibration amplitudes at lower spindle speeds.

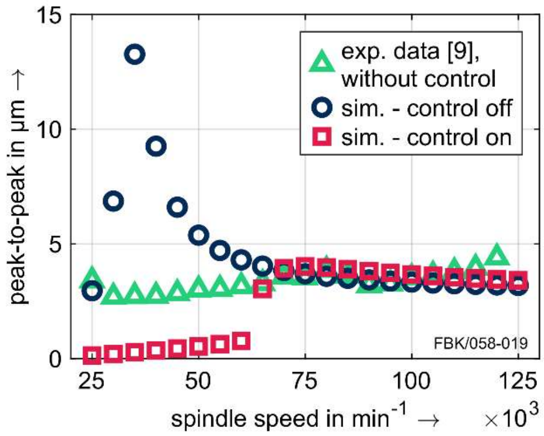

Figure 2. Comparison of peak-to-peak values of rotor vibration amplitudes as a function of the spindle speed for different scenarios

The simulated vibration amplitudes with active control exhibit two-part behavior with a transition range at approximately 65 000 min^{-1}. At low speeds, the peak-to-peak values range from 0.13 µm to 0.60 µm; at higher speeds, they closely match the vibration amplitudes of the uncontrolled spindle. In the transition range, the vibration amplitudes increase sharply, from 0.60 µm to 4 µm with a 10 000 min^{-1} speed increase.

A detailed analysis of the vibration amplitudes with and without enabled control system is shown in figure 3.

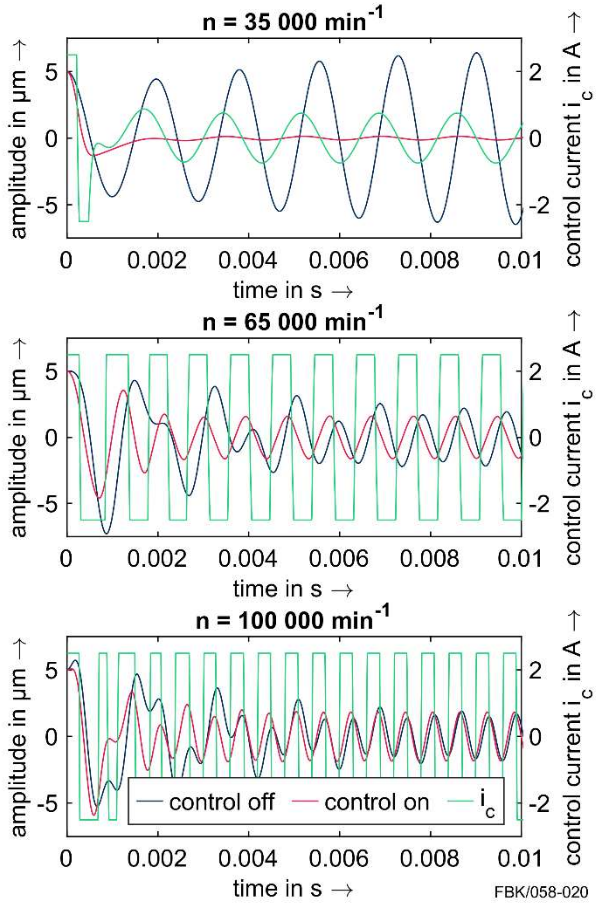

Figure 3. Comparison of the simulated vibration amplitudes for three spindle speeds

For the low spindle speed range – illustrated for n = 35 000 min^{-1} – the vibration control is able to compensate the rotor vibrations within the first revolution effectively by 98 %. The control current amplitude required for this compensation is approximately 0.75 A. For the high spindle speed range – illustrated for n = 100 000 min^{-1} – almost no vibration compensation is registered. After a brief settling phase that takes place over a few revolutions, the vibration amplitudes demonstrate almost identical curves. The control currents i_c fluctuate between the saturation limits of ± 2.5 A with the spindle speed. In case of the transition range – n = 65 000 min^{-1} – the vibration amplitudes are only slightly compensated. The corresponding control currents i_c already reach the compensation limit of ± 2.5 A. A notable difference compared to the high-speed behavior is the greater phase shift between unregulated and regulated vibration amplitudes.

4. Discussion

The results for the peak-to-peak values of the rotor vibrations for the whole operational spindle speed range confirmed that the chosen approach is capable of modeling the rotordynamics. Calculating the magnetic bearing forces and the air bearing forces numerically with finite element simulations enables accurate representation of the real system behavior. The low computational costs necessary for real-time control are ensured by implementing these results via lookup tables in the closed-loop control model. The experimental rotor vibration data is in close agreement with the simulated values. The larger deviation at lower spindle speeds, where the spindle speeds match a natural frequency in the simulation, overestimate the actual system response. Therefore, any conclusions drawn from this system model will lead to a conservative system design.

The detailed analysis of the system behavior in the three distinct speed ranges (figure 3) emphasizes the possibilities and limitations of the current control setup. Up until 60 000 min^{-1} the rotor vibrations can be supressed effectively by at least 75 %. In the following transition range the control currents reach their saturation limit. The induced magnetic forces are not high enough to compensate the rising unbalance forces and force the rotor into the setpoint position with just the feedback control. However, the imposed phase shift between the free and controlled rotor movement suggest that the control forces, i.e. magnetic forces, can significantly influence the rotor movement. Due to the nature of the feedback control environment the control system constantly trails the system response and imposes the phase shift. With advanced control schemes, e.g. feedforward approaches, the achievable control forces could be sufficient to also achieve substantial vibration suppression. Above 70 000 min^{-1} there is basically no change detectable in the system response despite the magnetic actuator forces.

5. Conclusion and Outlook

In this paper, we introduced a control system model for a micro machining spindle with an active magnetic bearing actuator. The simulation of the rotor dynamics is represented through the equations of motion for a lumped mass approach in three dimensions (positions x and y, angle about the z-axis φ). The magnetic bearing forces and the constant for the calculation of the air bearing forces (stiffness and damping coefficients) are determined numerically through three dimensional magnetostatic and two dimensional fluid dynamics finite element simulations. The results of these computationally intensive simulations is implemented via lookup tables in the closed-loop control system model setup in MATLAB Simulink.

A comparison of the control system response without active control and experimental rotor vibration data proved the validity of the model. The subsequent comparison with the closed-loop response (magnetic bearing actuator activated) proved the damping capabilities of the hybrid spindle setup: With the current setup, the system was capable of significantly suppressing rotor vibrations up to 60 000 min^{-1}. At higher spindle speeds the damping capabilities are limited by the feedback control approach and the maximum magnetic forces. While the rotor vibrations can not be suppressed at higher spindle speeds, the system remains stable.

In future work two limitations will be addressed:

- The lumped mass approach does not represent the geometric design and positioning of bearing forces, imbalances and external loads. The model will be extended to five degrees of freedom. With the additional equations of motion for the angles about the x- and y-axis the model can account for tilting of the rotor.
- Instead of strict feedback control, more advanced control strategies (e.g. feedforward control schemes) will be employed to enhance the damping capabilities at higher spindle speeds and decrease the necessary control interventions as much as possible.

Acknowledgment

This research was funded by the Deutsche Forschungsgemeinschaft (DFG, German Research Foundation) – 491400446.

[1]Naming of specific manufacturers is done solely for the sake of completeness and does not necessarily imply an endorsement of the named companies nor that the products are necessarily the best for the purpose.

References

[1] Balázs B Z, Geier N, Takács M and Davim J P 2021 A review on micro-milling: recent advances and future trends *Int J Adv Manuf Technol* **112** 655–684

[2] O'Toole L, Kang C-W and Fang F-Z 2021 Precision micro-milling process: state of the art *Advances in manufacturing* **9** 173–205

[3] Harris P, Wintterer M, Jasper D, Linke B, Brecher C and Spence S 2020 Design and Development of a High Efficiency Air Turbine Spindle for Small-Part Machining *Int. J. of Precis. Eng. and Manuf.-Green Tech.* **7** 915–928

[4] Sun Y, Wu Q, Chen W, Luo X and Chen G 2021 Influence of Unbalanced Electromagnetic Force and Air Supply Pressure Fluctuation in Air Bearing Spindles on Machining Surface Topography *Int. J. Precis. Eng. Manuf.* **22** 1–12

[5] Kimman M H, Langen H H and Munnig Schmidt R H 2010 A miniature milling spindle with Active Magnetic Bearings *Mechatronics* **20** 224–235

[6] Jang H-D, Kim J, Han D-C, Jang D-Y and Ahn H-J 2014 Improvement of high-speed stability of an aerostatic bearing-rotor system using an active magnetic bearing *Int. J. Precis. Eng. Manuf.* **15** 2565–2572

[7] Müller C, Greco S, Kirsch B and Aurich J C 2017 A Finite Element Analysis of Air Bearings Applied in Compact Air Bearing Spindles *Procedia CIRP* **58** 607–612

[8] Lange A, Müller D, Kirsch B and Aurich J C 2021 Numerical analysis of magnetic bearings for micro machining applications *Proc. euspen's 21st International Conference & Exhibition* (Bedford, UK: euspen) **21** 247–250

[9] Zell F, Lange A, Kirsch B and Aurich J C 2024 Analysis of the vibration characteristics of an air bearing spindle to identify and control the magnitude of the radial run-out with an active magnetic bearing *Proc. euspen's 24th International Conference & Exhibition* (Bedford, UK: euspen) **24** 449–452